Healing behavior of microcracks on the surface of yttria-stabilized polycrystals using an ultrafast high-temperature sintering method

Toshiki SATO[a], Ayu KODAIRA[a], Tomoharu TOKUNAGA[a], Koji MORITA[b], Takahisa YAMAMOTO[a, *]

[a] Department of Materials Design Innovation Engineering, Nagoya University, Furo-cho, Chikusa-ku, Nagoya, 464-8603, Japan

[b] Research Center for Electronic and Optical Materials, National Institute for Materials Science, Sengen 1-2-1, Tsukuba, Ibaraki 305-0047, Japan

Corresponding author: T. Yamamoto; E-mail: yamamoto.takahisa@material.nagoya-u.ac.jp

Keywords: UHS, microcrack healing, zirconia, Vickers, scanning transmission electron microscopy

Abstract

A technique to heal microcracks on ceramic surfaces in a relatively short time is an attractive proposition for extending the lifetime of ceramics. To this end, we used the ultrafast high-temperature sintering (UHS) method, which permits a rapid temperature increase, to heal Vickers indentation microcracks generated in a 4 mol% Y_2O_3-doped ZrO_2 polycrystal. We examined the microstructure following microcrack healing using transmission electron microscopy and scanning electron microscopy with continuous focused ion beam slicing along the microcrack plane. This revealed that the microcrack healing process involves crack pinching and neck formation, followed by the growth of the neck. The microcracks were fully healed at the surface by UHS treatment at 2000 °C for 20 s. However, residual pores corresponding to the unhealed state were observed inside the material. We hypothesized that these pore residues were caused by significant grain coarsening during UHS. It is essential to optimize the UHS temperature and time to account for grain coarsening and facilitate the application of this method to microcrack healing.

1. Introduction

Most ceramics exhibit brittle fracture behavior resulting from crack propagation [1]. The presence of surface microcracks can greatly limit the lifetime of ceramics. Therefore, the healing of surface microcracks is considered to be one of the most effective ways to extend the lifetime of ceramics [2]. The healing of microcracks in ceramics has long been performed by heat treatment, which needs long-term treatment at high temperature. To achieve healing effectively at low temperatures and in a short time, novel techniques have been developed. These include self-healing techniques, which heal surface microcracks using chemical reactions of glass-forming phases caused by healing aids [3,4], and anodic oxidation techniques, which heal microcracks at room temperature by electrochemically treating a pre-dispersed metallic phase [5]. The major advantage of these methods is that they can heal microcracks at the operating temperature of ceramics or at room temperature. However, to achieve healing using these techniques, the dispersion of a second phase to promote healing (i.e. a healing aid) is essential. This makes it necessary to adjust the composition and microstructure of the ceramic.

Morita et al. developed a flash healing method using a flash event [6-8], which, in contrast with the aforementioned methods, does not require modification using healing aids to achieve microcrack healing in a short time. This method uses a steep power spike caused by the flash event when an oxide ceramic is heated under an electric field above a threshold value, which even enhances mass diffusion over a very short time [9-14]. For example, they applied a flash healing method to Vickers indentation microcracks on the surface of stabilized zirconia polycrystals (8 mol% Y_2O_3-ZrO_2) as a model material and investigated the microcrack healing behavior under the flash event [6-8]. The degree of healing under an electric field of 50 V/cm was approximately 200 times higher than without the application of the electric field and heat treatment [7].

Recently, the ultrafast high-temperature sintering (UHS) method was developed [15]. This method uses carbon felt with a low heat capacity as the heating source, enabling temperatures to be raised to as high as 2000 °C in a few seconds. The UHS method has been widely applied to several high-temperature processing [16] owing to its advantages a short sintering time [17, 18] and/or suppression of volatile decomposition [19]. Using the UHS method, it is expected that the healing time of microcracks on ceramic surfaces can also be completed in a short time even in the absence of an electric field. In this study,

we applied the UHS method to heal Vickers indentation microcracks generated on a surface of partially stabilized zirconia doped with 4 mol% Y_2O_3 as a model ceramic [20]. We discuss the effectiveness of the UHS method as a microcrack healing technique.

2. Materials and Methods

4 mol% Y_2O_3-doped ZrO_2 (4YSZ) sintered polycrystals were used for UHS treatment to heal Vickers microcracks. Commercially available 4YSZ powder (Toso Co., Ltd., Japan) was used as the raw material. Green compacts with dimensions of approximately 3.5 × 3.5 × 15 mm^3 were fabricated by a conventional pressing method, including a cold-isostatic press. After pressing, the green compacts were sintered in air at 1400 °C for 3 h using an electric furnace, in which the relative density of the sintered compact was approximately 99%.

The samples used for microcrack healing were machined from the sintered compacts to dimensions of 3 × 3 × 0.5 mm^3, in which the planes with 3 × 3 mm^2 were mechanically polished to a mirror state using a diamond slurry. After polishing, to remove the residual stress caused by mechanical polishing, the polished samples were annealed at 1100 °C for 0.5 h in air according to a previous report [6]. The average grain size of the sintered 4YSZ polycrystal was approximately 0.41 μm. The microcracks were generated on the mirror-finished surfaces by the indentation method using a micro-Vickers indenter (Via-S, Matsuzawa Co., Ltd.) at a load of 1000 gf applied for 15 s.

After indentation, the samples were treated using the UHS method with a hand-made apparatus, as illustrated in Figure 1(a). Copper electrodes, to which carbon felt (GF-20-2FSH, Nippon Carbon Corp.) were fixed, were installed inside the vacuum chamber. The samples were inserted in the space between the upper and lower carbon felt, as shown in Fig.1 (a). Electric power to the carbon felt sheets was supplied by a direct current (DC) power supply (PWR1201ML, Kikusui Electronics Industries, Ltd.,) in a current-control mode. The surface temperature of the upper carbon felt was measured using a radiation thermometer (FTKX-TNE0240-0500H101-000, Japan Sensor Corp.). The current in the carbon felt was computer-controlled, and the current and surface temperature of the carbon felt during UHS treatment were recorded with a data logger. The sample temperatures (inside temperature between upper and lower carbon felts) were calculated using simulation software that uses the finite element method (Autodesk Inventor Professional 2025, Autodesk Inc.). For this purpose, the parameters of thermal conductivity and specific heat of the carbon felts were set during the simulation so that the surface temperature of the upper carbon felt measured with a radiation thermometer would match the calculated temperature obtained in the simulation (Fig. 1(b)). The

accuracy of these settings was confirmed using the melting point of platinum wire inserted at the space used for sample setting between upper and lower carbon felts. Based on these settings, the temperature between the two carbon felt (sample temperature) was calculated, as shown in the colored lines labeled with 1600, 1800, and 2000 °C in Fig. 1 (b). The time from the onset of the temperature rise to the end of UHS treatment was varied in the range of 5–20 s for sample temperatures of 1600–2000 °C, and the rate of temperature rise during UHS treatment was approximately 2000 °C/min. The holding time at the maximum temperature was 0–15 s.

The surface morphology in the vicinity of the indents was observed using an optical microscope (Nikon Corp. ECLIPSE LV100ND) and a scanning electron microscope equipped with a focused ion beam (FIB-SEM; MI4000L, Hitachi High-Tech Corp.) under a low acceleration voltage of 1 kV. For the sample treated with UHS at 2000 °C for 5 s, a series of SEM images was captured using continuous FIB slicing, with slices taken every 15 nm in thickness. In addition, the microstructure along a healed microcrack inside the sample treated with UHS at 2000 °C for 20 s was observed using scanning transmission electron microscopy (STEM, ARM-200FC, JEOL Ltd.) at an acceleration voltage of 200 kV. STEM thin foils were prepared using FIB-SEM. FIB pick-up was conducted to allow STEM observation in the direction parallel to the original microcrack plane.

3. Results

Figure 2 shows SEM images taken from (a) a Vickers indentation on the sample surface, (b) a microcrack that generated from the corner of the indentation, and (c) an enlarged image of the dotted white rectangular area shown in (b). As shown in Fig. 2(a), the microcracks propagated roughly in a straight manner from the corner of the indentation. The average length of the microcracks, l_0, was approximately 19.8 μm, and the average diagonal length of the indentation, a, was approximately 26.7 μm. The fracture toughness, K_{IC}, and Vickers hardness, Hv, from the Vickers indentation method were obtained using the following equations [21]

$$K_{IC} = 0.016\left(\frac{E}{H_V}\right)^{0.5}\left(\frac{P}{c^{1.5}}\right)$$

$$H_V = 0.1891\left(\frac{P}{a^2}\right)$$

where E is Yang's modulus, c is the half-length of the averaged microcrack length (Fig. 2(a)), a is the averaged diagonal length of indent (Fig. 2(a)), and P is the load of the indentation. For the value of E, 205 GPa, which has been reported previously for 4YSZ polycrystals, was used [22]. The fracture toughness and Vickers hardness were calculated to be 1372 N/mm and 3.53, respectively. These values were approximately comparable to those previously reported for 4YSZ polycrystals [22].

As shown in the magnified image in Fig. 2(c), microcracks on the surface propagated mainly along the grain boundaries, but also within the grains for the larger grains. The microcrack width decreased from approximately 200 nm near the indentation to the microcrack tip. The morphology of the microcracks produced by the Vickers indentation test was almost similar to that reported previously [6-8,23].

Figure 3 shows SEM images of the microcrack surface after UHS treatment at 2000 °C for 5–20 s. Here, the UHS treatment time is described as the time from the start of the sample temperature rise to the end of treatment (Fig. 1(b)). Figure 3(a) shows the microcracks before UHS treatment (Fig. 2(b)) for comparison, in which the microcrack length was approximately 21 μm. After UHS treatment at 2000 °C, the microcrack length decreased with treatment time. The microcracks were almost completely healed on the surface even after a treatment time of just 20 s (Fig. 3(d)), including the time required to raise the temperature from room temperature to the UHS treatment temperature.

Figure 4 shows the healing ratio for treatment at 1600–2000 °C as a function of treatment time. The healing ratio, H_t is defined as [6]:

$$H_t = \frac{\Delta l}{l_0} = \frac{(l_0 - l_t)}{l_0}$$

where l_0 and l_t are the length of microcrack before and after UHS treatment, respectively, and $\Delta l = (l_0 - l_t)$ (see Fig. 3(a) and (b)). The healing ratio increased in all cases with UHS treatment temperature and time (Fig. 4).

Figure 5(a) shows SEM images of the FIB-sliced surface near the microcrack of the sample treated at 2000 °C for 5 s, and Fig. 5 (b–h) shows a series of SEM images obtained through continuous FIB slicing, with each slice approximately 15 nm in thickness. Continuous FIB slicing was performed from approximately 5 μm from the corner of the indentation (indicated by the white triangle in Fig. 3(c)) and in the direction of the indentation. The image in Fig. 5(a) is rotated 90 degrees to show a wide field of view.

After 5 s of UHS treatment, microcracks were healed in the vicinity of the sample surface (white arrows in Fig. 5(a)), but remained in the wide area inside the sample with their width decreasing from the near the surface to the interior. The cross-sectional images in Fig. 5(b)–(h) were obtained from the area indicated by the white dotted square in Fig. 5(a). These images confirm that the microcrack healing process was caused by neck formation due to crack pinching between the inner surfaces of the microcrack and the growth of the neck. For example, near arrow A in Fig. 5(d), the microcrack is open, but near arrow A in Fig. 5(c), it's inner surface on the right side protrudes convexly toward the opposing inner surface to form a neck. This contact between microcrack surfaces during the healing process is similar to the microstructure previously reported as "crack pinching" [24,25]. At arrow A in Fig. 5(b), the neck area formed by the convex overhang grew. The process of neck formation by crack pinching and its growth were also confirmed from the microstructural changes in the areas indicated by arrows B and C. Arrow B in Fig. 5(h) shows the contact point of the microcrack inner surfaces as described above (similar at arrow A in Fig. 5(c)). From this point, the neck can be seen to grow in the direction of arrow C in Fig. 5(g) to (c). This neck growth is caused by the small curvature at the neck, which is a similar phenomenon to that observed in the sintering process [26]. As a result, an isolated pore is formed at the location indicated by arrow D in Fig. 5(b). Similar healing processes can be observed at the locations indicated by arrow E and F. The results in Fig. 5 suggest that microcrack healing using UHS treatment progresses by neck formation and subsequent neck growth caused by convex structures formed from the inner surfaces of the cracks.

Figure 6 shows the microstructural observation results for the sample after UHS treatment at 2000 °C for 20 s. STEM thin foil was prepared by slicing, picking up, and thinning from the region near the indentation corner using FIB for STEM observation in the direction parallel to the original microcrack plane. As shown in the bright-field STEM image (Fig. 6(a)), although the area near the surface of the microcrack had completely healed, pores with diameters ranging from approximately 100 to 300 nm formed inside the sample.

After UHS treatment, the 4YSZ polycrystal exhibited a tetragonal single phase with a c/a-axis ratio of 1.01 (a = 0.511 nm, c = 0.517 nm), as indicated in the selected area diffraction (SAD) pattern, which was acquired to include grains on both sides of the

aligned pores (Fig. 6(b)). The SAD pattern also revealed forbidden diffraction spots due to the tetragonal symmetry, as indicated by the arrows [27]. This tetragonality (*c*/*a*-axis ratio) was similar to that of previously reported for 4YSZ polycrystals [28]. The tetragonal–cubic phase separation, which is shown in the ZrO_2-Y_2O_3 pseudo binary phase diagram, did not occur after UHS treatment because of its very short duration even at 2000 ℃ [29, 30]. No separation or elongation were observed in the diffraction spots in the SAD pattern of Fig. 6(b). This confirms that the grains on both sides of the residual pores were completely aligned in a single-crystal orientation relationship. In addition, the residual pores were observed to be a hexagonal shape with a specific crystalline habit plane (Fig. 6(c)). The habit planes in the pores remaining inside the sample after UHS treatment are similar to those of the residual pores after the healing of microcracks formed on the surface of a zirconia single previously [31, 32]. From the SAD pattern (Fig. 6(b)), we confirmed that the habit planes constituting the inner surfaces of the pores were {111} and (100) (Fig. 5(c)). Both habit planes correspond to those with lower surface energy in cubic zirconia [33, 34].

4. Discussion

We previously investigated the thermal healing behavior of Vickers indentation microcracks generated on the (001) surface of zirconia single crystals [35]. We found that this healing process involves the recovery of high-density dislocations introduced during Vickers indentation. Dislocations that open microcracks are recovered with heat treatment, which releases the stress that opens the microcracks. The microcracks then closes by the recovery of dislocations. As the microcracks close, their inner surfaces come into contact with each other, forming a neck at the contact points. After that, microcrack healing proceeds by neck growth during heat treatment.

For polycrystalline materials, microcracks cannot be completely closed at high temperatures because of the complexity of the microcrack morphology. The healing process is schematically shown in Fig. 8. When an open microcrack is heated to a high temperature, its inner surface destabilizes and changes to a convex shape, subsequently making contact with the opposing inner surface of the crack (black arrows in Figs. 8(b) and 8(d)) [36, 37]. This phenomenon is called crack pinching, which contributes significantly to the formation of the neck in the early stages of healing [24, 25, 38]. After the neck is formed, healing proceeds by neck growth (arrows in Fig. 8(c–e)) similar to the process described above. As shown in Fig. 5, a healing process of crack pinching, neck formation, and neck growth can be considered to take place under UHS treatment.

One of the characteristics of the UHS method is its rapid temperature rise, which likely enhances mass diffusion. For example, there is significant densification during UHS despite its extremely short time [15-18]. In one study, Guo et al. found that the activation energy of sintering decreases during UHS, as revealed by their master-sintering curve analysis [39]. They described that the enhancement of mass diffusion during UHS is related to a non-equilibrium state at grain boundaries caused by rapid heating. This non-equilibrium state they claimed can be considered to have an significant influence on the rate of grain growth during UHS treatment. In the present study, the grain size rapidly increased from approximately 0.41 to 75 μm upon treatment at 2000 °C for 20 s (see a grain size shown in Fig. 3(d)). For example, in a study of grain growth behavior of 8YSZ polycrystals, Yoshizawa et al. found that the grain size increased only from approximately 7.5 μm to approximately 20 μm, even after heat treatment at 1800 °C for 12 h [40]. This grain growth rate is much smaller than that observed in the present study for UHS

treatment. The rapid surface healing of UHS treatment is inferred to be caused by the effect of enhanced mass diffusion during the rapid temperature increase, which Guo et al. claimed [39].

Complete healing of microcracks requires the eventual annihilation of the isolated pores generated by neck growth. We previously reported that annihilation of these pores is closely related to the distance between the pores and the grain boundaries in 8YSZ polycrystals [7]. The degree of healing decreased with increasing grain size, with healing being approximately one-tenth as effective for a grain size of 5.4 μm as for a grain size of 0.8 μm. The decrease in the degree of healing with coarser grains is due to the greater distance for slow lattice diffusion, which is necessary for pore elimination. Therefore, for polycrystals with coarse grains, the pores near grain boundaries are easily annihilated, but those inside the grains tend to remain. As shown in Fig. 5, even under conditions where microcracks were completely healed on the surface, residual pores corresponding to the unhealed state were observed inside the sample. This is because the grain size of the sample increased significantly to approximately 75 μm after UHS treatment. To apply UHS treatment to microcrack healing, it is essential to optimize the UHS treatment conditions, considering the grain growth rate.

5. Conclusions

We used the UHS method to heal Vickers microcracks formed on the surface of 4 mol% Y_2O_3-ZrO_2 polycrystal samples. We investigated the dependence of the degree of healing and the microstructure of the healed microcracks on the UHS treatment temperature and duration. The main findings are as follows.

1) After UHS treatment at 1600–2000 °C for 5–20 s, microcracks were healed, with a higher degree of healing observed at higher temperatures and for longer treatment times. At 2000 °C for 20 s, the microcracks on the sample surface were almost completely healed.

2) Continuous FIB slicing revealed that microcrack pinching occurred during the early stages of healing, where part of the inner microcrack surface transformed into a convex shape, creating a neck that made contact with the opposing inner surface of the crack. Microcrack healing by UHS treatment can be considered to proceed by the successive processes of crack pinching, neck formation, and neck growth.

3) The surface was completely healed by UHS treatment at 2000 °C for 20 s. However, residual pores with diameters ranging from 100 to 300 nm remained inside the sample. These pores were hexagonal in shape surrounded by low-surface-energy habit planes. We attribute the residual pores to grain size coarsening caused by UHS treatment. To effectively apply UHS treatment for microcrack healing, it is essential to optimize the treatment conditions while accounting for the grain size coarsening.

Acknowledgments

This work was financially supported by CREST (JPMJCR1996) from the Japan Science and Technology Agency.

References

[1] A.G. Evans, Perspective on the development of high-toughness ceramics, J. Am. Ceram. Soc., 73 (1990) 187–206, https://doi.org/10.1111/j.1151-2916.1990.tb06493.x.

[2] F. Tavangarian, D. Hui, G. Li, Crack-healing in ceramics, Compos. B. Eng., 144 (2018) 56–87, https://doi.org/10.1016/j.compositesb.2018.02.025.

[3] P. Greil, Self-healing engineering ceramics with oxidation-induced crack repair, Adv. Eng. Mater., 22 (2020) 1901121, https://doi.org/10.1002/adem.201901121.

[4] R. Dallaev, Advances in materials with self-healing properties: a brief review, Materials 17 (2024) 2464. https://doi.org/10.3390/ma17102464.

[5] S. Shi, T. Goto, S. H. Cho, T. Sekino, Electrochemically assisted room‐temperature crack healing of ceramic‐based composites, J. Am. Ceram. Soc., 102 (2019) 4236–4246, https://doi.org/10.1111/jace.16264.

[6] K. Morita, F. Naito and D. Terada: Microcrack healing in zirconia ceramics under a DC electric field/current, J. Eur. Ceram. Soc. 41 (2021) 282-289, https://doi:10.1016/j.jeurceramsoc.2021.09.044.

[7] S. Takahashi, K. Morita, K. Nambu, D. Terada, K. Kobayashi, T. Tokunaga, T. Yamamoto, Effect of initial grain size on crack healing behavior under DC electric field of zirconia (8Y-CSZ) Ceramic, Adv. Eng. Mater., 25 (2023) 2201807, https://doi.org/10.1002/adem.202201807

[8] S. Kawabata, S. Takahashi, K. Nambu, K. Morita, Effect of DC and AC electric fields on crack healing behavior in 8 mol% yttria-stabilized cubic zirconia polycrystal, J. Am. Ceram. Soc. 106 (2023) 6163–6176, https://doi.org/10.1111/jace.19269.

[9] M. Cologna, B. Rashkova, R. Raj, Flash sintering of nanograin zirconia in <5 s at 850◦C, J. Am. Ceram. Soc., 93 (2010) 3556–3559, https://doi.org/10.1111/j.1551-2916.2010.04089.x.

[10] M. Yu, S. Grasso, R. Mckinnon, T. Saunders, M.J. Reece, Review of flash sintering: materials, mechanisms and modelling, Adv. Appl. Ceram., 116 (2017) 24–60, https://doi.org/10.1080/17436753.2016.1251051.

[11] O. Guillon, R.A. De Souza, T.P. Mishra, W. Rheinheimer, Electric-field-assisted processing of ceramics: nonthermal effects and related mechanisms, MRS Bull., 46 (2021) 52–58, https://doi.org/10.1557/s43577-020-00008-w.

[12] K. Ren, Q.K. Wang, Y.L. Lian, Y.G. Wang, Densification kinetics of flash sintered 3mol% Y_2O_3 stabilized zirconia, J. Alloy. Compd., 747 (2018) 1073–1077, https://doi.org/10.1016/j.jallcom.2018.02.308.

[13] K. Nambu, T. Kitaoka, K. Morita, K. Soga, T. Tokunaga, T. Yamamoto, H. Masuda, H. Yoshida, Flash self-joining of Y-TZP ceramics assisted with an AC electric field, J. Am. Ceram. Soc., 106 (2023) 2073–2082, https://doi.org/10.1111/jace.18889.

[14] M. Koike, A. Kodaira, T. Tokunaga, T. Yamamoto, Apparent sintering activation energy estimated by master sintering curves for 8 mol% Y_2O_3 doped ZrO_2 polycrystals during shrinkage-rate controlled flash sintering, Mater. Trans., 64 (2023) 2315-2320, https://doi.org/10.2320/matertrans.MT-M2023048.

[15] C. Wang, W. Ping, Q. Bai, H. Cui, R. Hensleigh, R. Wang, A. H. Brozena, Z. Xu, J. Dai, Y. Pei, C. Zheng, G. Pastel, J. Gao, X. Wang, H. Wang, J.C. Zhao, B. Yang, X. Zheng, J. Luo, Y. Mo, B. Dunn, L. Hu, A general method to synthesize and sinter bulk ceramics in seconds, Science 368 (2020) 521–526 (2020), https://doi.org/10.1126/science.aaz7681.

[16] M. Kermani, C. Hu, S. Grasso, From pit fire to ultrafast high-temperature sintering (UHS): A review on ultrarapid consolidation, Ceram. Inter., 49 (2023) 4017–4029, https://doi.org/10.1016/j.ceramint.2022.11.091.

[17] R. Murakami, B. Feng, K. Matsui, S. Kondo, N. Shibata, Y. Ikuhara, Fabrication of 3YSZ with single tetragonal phase by ultrafast high-temperature sintering, Ceram. Inter., 50 (2024) 37308–37313, https://doi.org/10.1016/j.ceramint.2024.04.118.

[18] B. Zhang, M. Hu, F. Zhong, S. Zhang, Z. Yang, X. Qiu, J. Xu, J. O. Yang, Y. Zhang, B. Zhu, X. Yang, S. Chen, Ultrafast high-temperature sintering and densification of ZrC-based ceramics, J. Euro. Ceram. Soc., 44 (2024) 5569–5578, https://doi.org/10.1016/j.jeurceramsoc.2024.03.037.

[19] X. Kong, R. Gu, Z. Jin, L. Zhang, C. Zhang, W. Xiang, C. Li, K. Zhu, Y. Xu, H. Huang, X. Liu, R. Peng, C. Wang, Maximizing interface stability in all-solid state lithium batteries through entropy stabilization and fast kinetics, Nature Comm., 15 (2024) 7247, https://doi.org/10.1038/s41467-024-51123-0.

[20] M. Ciszynski, B. Chwaliszewski, W. Simka, M. Dominiak, T. Gedrange, J. Hadzik, Zirconia dental implant designs and surface modifications: a narrative review, Materials 17 (2024) 4202, https://doi.org/10.3390/ma17174202.

[21] G.R. Anstis, P. Chantikul, B.R. Lawn, D.B. Marshall, A critical evaluation of indentation techniques for measuring fracture toughness: I, direct crack measurements, J. Am. Ceram. Soc. 64 (1981) 533–538, https://doi.org/10.1111/j.1151-2916.1981.tb10320.x.

[22] V.V. Kulyk, Z.A. Duriagina, B.D. Vasyliv, V.I. Vavrukh, P. Ya. Lyutyy, T.M. Kovbasiuk, M.Y. Holovchuk, Effects of yttria content and sintering temperature on the microstructure and tendency to brittle fracture of yttria-stabilized zirconia, Archives of Materials Science and Engineering 109 (2021) 65-79, https://doi.org/10.5604/01.3001.0015.2625.

[23] G. A. Gogotsi, S. N. Dub, E. E. Lomonova, B. I. Ozersky, Vickers and knoop indentation behaviour of cubic and partially stabilized zirconia crystals, J. Euro. Ceram. Soc., 15 (1995) 405-413, https://doi.org/10.1016/0955-2219(95)91431-M.

[24] B. A. Wilson, E. D. Case, In situ microscopy of crack healing in borosilicate glass, J. Mater. Sci., 32 (1997) 3163-3175, https://doi.org/10.1023/A:1018698600884.

[25] T.K. Gupta, Crack healing in thermally shocked MgO, 58 (1975) 143-143, https://doi.org/10.1111/j.1151-2916.1975.tb19578.x.

[26] Z. Liu, Q. Cheng, Y. Wang, Y. Li, J. Zhang, Sintering neck growth mechanism of Fe nanoparticles: A molecular dynamics simulation, Chem. Eng. Sci., 218 (2020) 115583, https://doi.org/10.1016/j.ces.2020.115583.

[27] T. Sakuma, Y. Yoshizawa, H. Suto, The metastable two-phase region in the zirconia-rich part of the ZrO_2-Y_2O_3 system, J. Mater. Sci., 21 (1986) 1436-1440, https://doi.org/10.1007/BF00553285.

[28] N. Shibata, J. Katamura, A. Kuwabara, Y. Ikuhara, T. Sakuma, The instability and resulting phase transition of cubic zirconia, Mater. Sci. Eng., A312 (2001) 90–98, https://doi.org/10.1016/S0921-5093(00)01863-3.

[29] E. R. Andrievskaya, V. V. Kovylyaev, L. M. Lopato, A. V. Shevchenko, A. A. Frolov, Liquidus surface of the ZrO_2–Y_2O_3–Eu_2O_3 phase diagram, Powder Metall. Met. Ceram., 53 (2014) 312-322, https://doi.org/10.1007/s11106-014-9618-y.

[30] K. Matsui, H. Yoshida, Y. Ikuhara, Isothermal sintering effects on phase separation and grain growth in yttria-stabilized tetragonal zirconia polycrystal, J. Am. Ceram. Soc., 92 (2009) 467-475, https://doi.org/10.1111/j.1551-2916.2008.02861.x.

[31] S. Kayukawa, Y. Katsuyama, A. Kodaira, T. Tokunaga, K. Morita, A. Nakamura, T. Yamamoto, Flash healing of Vickers microcracks formed on the (001) surface of cubic zirconia single crystals, J. Euro. Ceram. Soc., 43 (2023) 6272–6278, https://doi.org/10.1016/j.jeurceramsoc.2023.06.001.

[32] S. Kayukawa, Y. Katsuyama, A. Kodaira, T. Tokunaga, K. Morita, T. Yamamoto, Microstructural analysis of flash-healed Vickers-indented microcracks near positive/negative electrodes on the (001) surface of cubic zirconia single crystals under direct current electric fields, Ceram. Inter., 50 (2024) 37348-37355, https://doi.org/10.1016/j.ceramint.2024.04.251.

[33] A. Christensen, E.A. Carter, First-principles study of the surfaces of zirconia, Phys. Rev. B, 58 (1998) 8050–8064, https://doi.org/10.1103/PhysRevB.58.8050.

[34] G. Ballabio, M. Bernasconi, F. Pietrucci, S. Serra, Ab initio study of yttria-stabilized cubic zirconia surfaces, Phys. Rev. B, 70 (2004) 075417, https://doi.org/10.1103/PhysRevB.70.075417.

[35] S. Kayukawa, Y. Katsuyama, A. Kodaira, T. Tokunaga, K. Morita, A. Nakamura, K. Higuchi, T. Yamamoto, Microcrack healing in single-crystal cubic zirconia by thermal annealing, J. Eur. Ceram. Soc., 43 (2023) 1078–1086, https://doi.org/10.1016/j.jeurceramsoc.2022.10.065.

[36] T.K. Gupta, Instability of cylindrical voids in alumina, J. Am. Ceram. Soc. 61 (1978) 191–195, https://doi.org/10.1111/j.1151-2916.1978.tb09276.x.

[37] F.A. Nichols, On the spheroidization of rod-shaped particles of finite length, J. Mater. Sci., 11 (1976) 1077–1082, https://doi.org/10.1007/BF02396641.

[38] T.K. Gupta, Crack healing and strengthening of thermally shocked alumina, J. Am. Ceram. Soc., 59 (1976) 259–262, https://doi.org/10.1111/j.1151-2916.1976.tb10949.x

[39] Z. Guo, R. Todd, Acceleration of grain boundary diffusion during ultrafast high-temperature sintering (UHS) of alumina powder compacts, Acta Mater., (2024) (under review, Guo, Zonghao and Todd, Richard, Acceleration of Grain Boundary Diffusion During Ultrafast High-Temperature Sintering (UHS) of Alumina Powder Compacts. available at SSRN: https://ssrn.com/abstract=4917372).

[40] Y. Yoshizawa, T. Sakuma, Evolution of microstructure and grain growth in ZrO_2-Y_2O_3 alloys, ISIJ International, 29 (1989) 746-752, https://doi.org/10.2355/isijinternational.29.746.

Figures and Captions

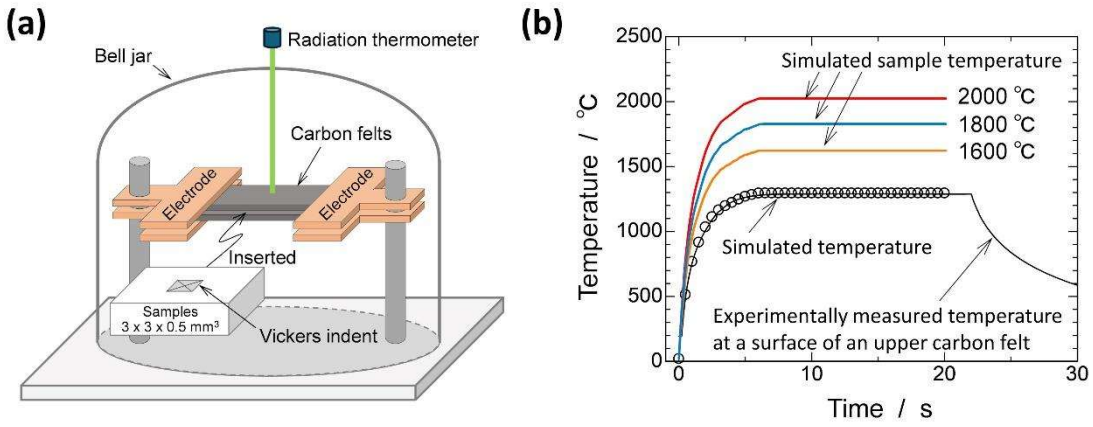

FIGURE 1 (a) Schematic illustration of the set-up for UHS treatment. (b) Measured and simulated temperatures at the surface of the upper carbon felt, and the simulated sample temperature (a space between upper/lower carbon felts where samples are inserted) as functions of time.

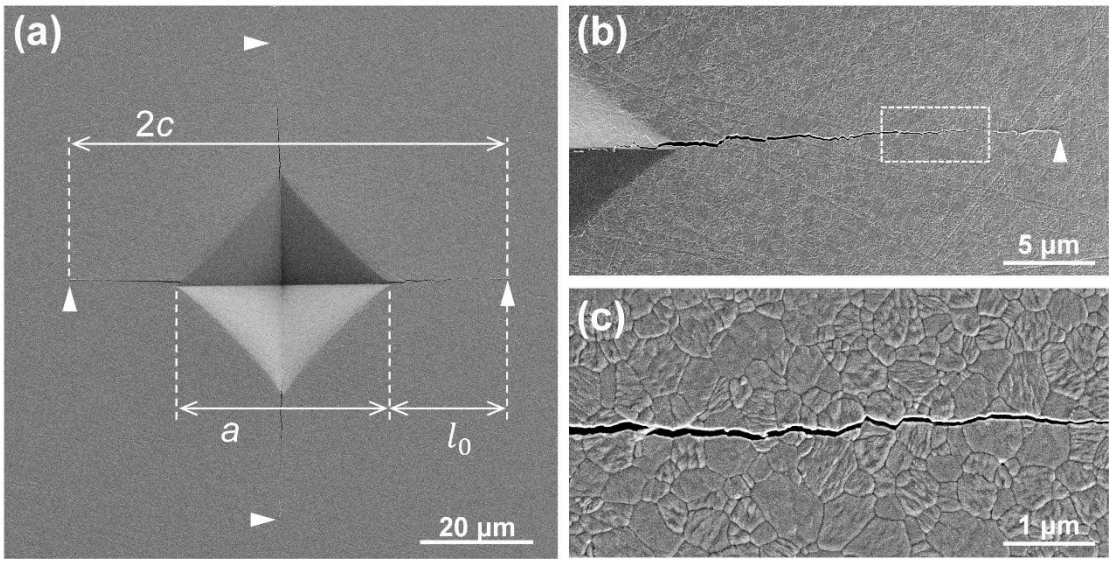

FIGURE 2 SEM images of (a) a pristine Vickers indentation, including microcracks formed from the corners of the indentation, (b) a microcrack, and (c) a magnified microcrack at the area indicated by the white dotted box in (b). The white triangles indicate the tips of the microcracks. The notations $2c$, a, and l_0 in (a) are described in the text.

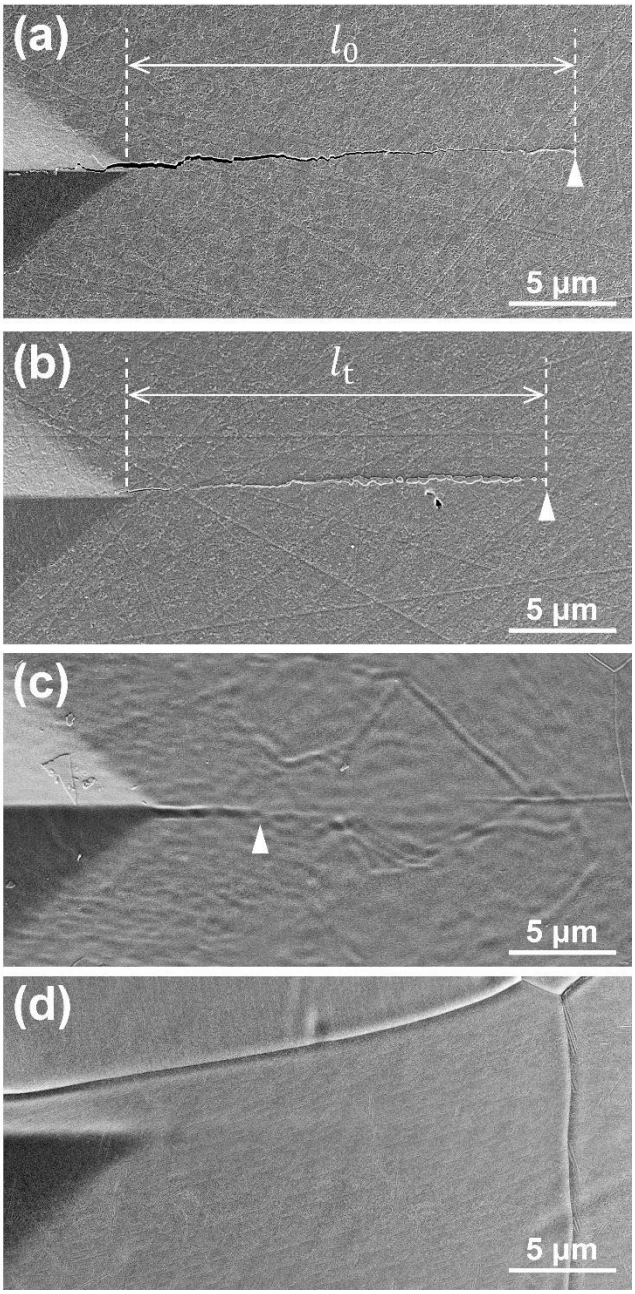

FIGURE 3 SEM images of microcracks from (a) a pristine Vickers indentation and (b–d) samples after UHS treatment at 2000 °C for 5, 10, and 20 s, respectively. The white triangles indicate the tips of the microcracks. The notations l_0 and l_t in (a) and (b) are described in the text.

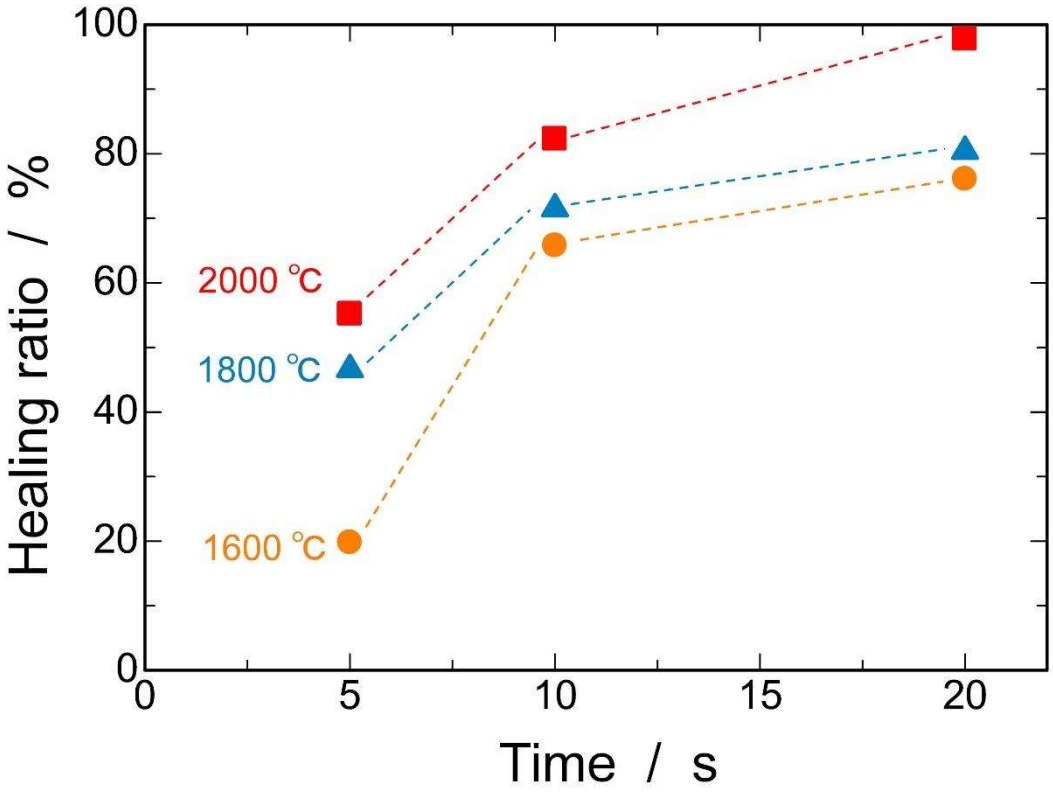

FIGURE 4 Healing ratio, H_t, after UHS treatment at 2000 °C (red dots), 1800 °C (blue dots), and 1600 °C (orange dots) as a function of time.

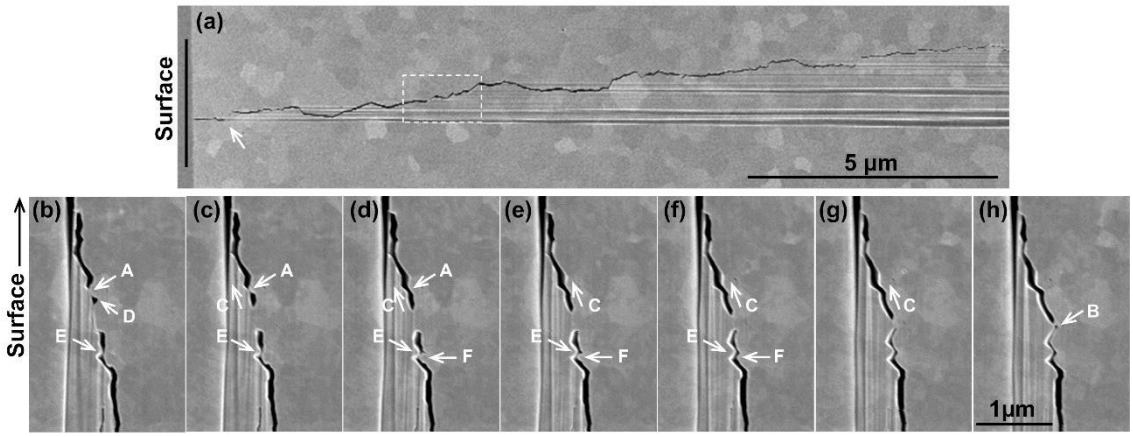

FIGURE 5 (a) SEM image showing a wide field of view of a microcrack in the sample after UHS treatment at 2000 °C for 5 s. (b–h) SEM images acquired every 15 nm in thickness by continuous FIB slicing. These images were taken from the area indicated by the white dotted box in (a). Note that (a) is rotated 90 degrees to the left.

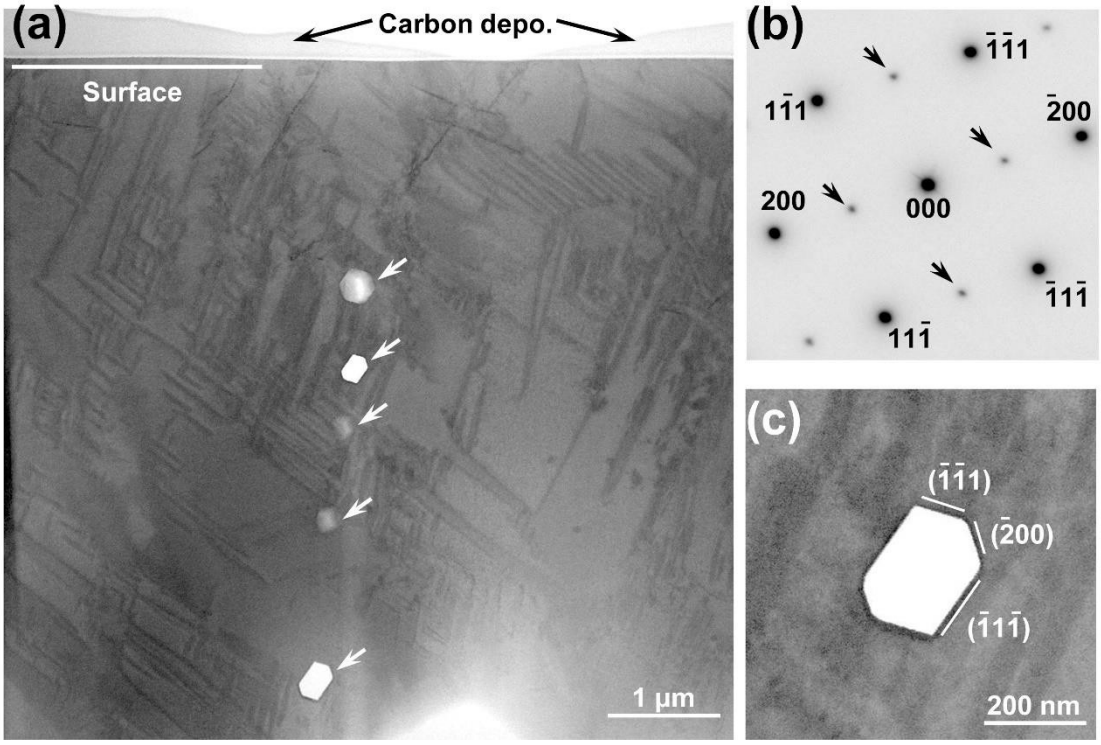

FIGURE 6 (a) BF-STEM image of a healed microcrack of after UHS treatment at 2000 °C for 20 s. (b) SAD pattern including crystal regions on both sides of a row of residual pores. (c) Magnified BF-STEM image of a residual pore.

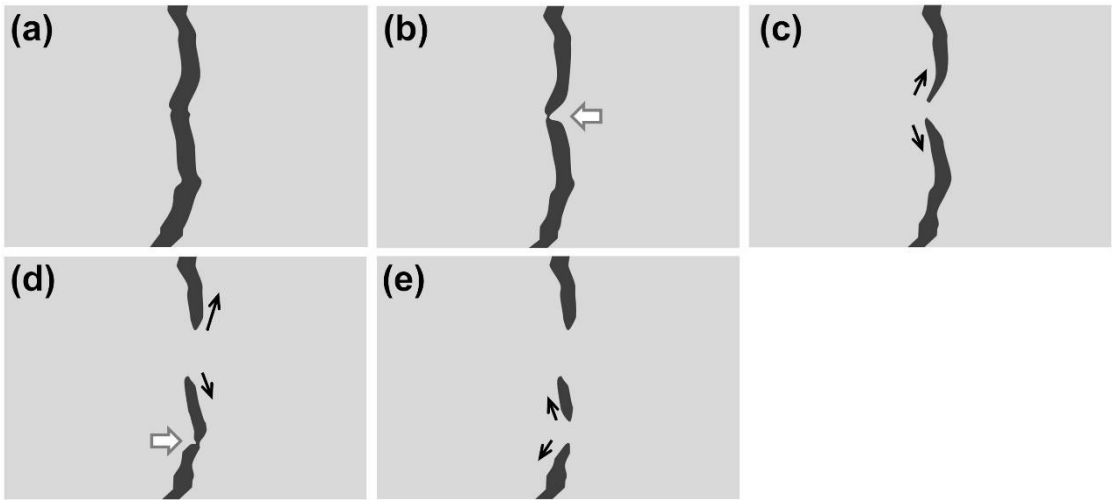

FIGURE 7 Schematic illustration of the microcrack healing process during UHS treatment.

Declaration of Interest Statement

Declaration of interests

☒ The authors declare that they have no known competing financial interests or personal relationships that could have appeared to influence the work reported in this paper.

☐ The author is an Editorial Board Member/Editor-in-Chief/Associate Editor/Guest Editor for *[Journal name]* and was not involved in the editorial review or the decision to publish this article.

☐ The authors declare the following financial interests/personal relationships which may be considered as potential competing interests: